# Fire hazards of carbonate-based electrolytes for sodium-ion batteries: What changes from lithium-ion batteries?

Pempa Tshering Bhutia, Sylvie Grugeon, Jean-Pierre Bertrand, Ghislain Binotto, Arnaud Bordes, Asmae El Mejdoubi, Stéphane Laruelle, Guy Marlair

Journal of Power Sources 622 (2024) 235234

Contents lists available at ScienceDirect

Journal of Power Sources

journal homepage: www.elsevier.com/locate/jpowsour

# Fire hazards of carbonate-based electrolytes for sodium-ion batteries: What changes from lithium-ion batteries?

Pempa Tshering Bhutia [a,b,c,d], Sylvie Grugeon [b,c], Jean-Pierre Bertrand [a], Ghislain Binotto [a], Arnaud Bordes [a], Asmae El Mejdoubi [e], Stéphane Laruelle [b,c], Guy Marlair [a,*]

[a] Institut National de l'Environnement Industriel et des Risques (INERIS), Parc Technologique Alata, BP2, 60550, Verneuil-en-Halatte, France
[b] Laboratoire de Réactivité et Chimie des Solides, CNRS UMR 7314, Université de Picardie Jules Verne, Amiens, 80039, France
[c] RS2E, Réseau Français sur le Stockage Electrochimique de l'Energie, FR CNRS 3459, CEDEX 1, F-80039, Amiens, France
[d] Alistore-European Research Institute (ERI), FR CNRS 3104, F-80039, Amiens Cedex 1, France
[e] TIAMAT, 72 rue des Jacobins, 80000, Amiens, France

## HIGHLIGHTS

- Fire behavior of Na-ion electrolytes with and without additives were studied.
- A comparison was established with classical Li-ion electrolyte.
- Heat release rate revealed mainly governed by the solvent components.
- Chemical threat influenced by salts and additives, and ventilation degree.
- Fluorine fate of Na-ion and Li-ion electrolytes reveals a quite different trend.

## ARTICLE INFO

*Keywords:*
Na-ion battery
Electrolyte
Additives
Fire propagation apparatus
Heat release rate
Toxic gas

## ABSTRACT

Carbonate-based electrolytes are often employed as the preferred electrolyte for both Li-ion and Na-ion cells. To investigate the fire risk during abuse conditions in real-life scenarios covering the full value chain, not only cell-level studies but also component-level investigation is crucial. Hence, Na-ion advanced electrolyte combustion tests are performed employing the fire propagation apparatus also called Tewarson calorimeter. Heat and combustion products releases are measured, making use of fire calorimetry laws and analytical techniques such as FTIR, NDIR, FID, or paramagnetic analyzers, and optical measurement. Thermal and chemical impacts of Na-ion electrolytes combustion and fires are assessed under well-ventilated and under-ventilated environments. Data are then compared against a carbonate-based electrolyte used in Li-ion batteries to create a comparative study between these technologies. Overall, the heat released rate majorly depends upon the solvents used and is less impacted by inorganic Li or Na salts while the emitted gases depend on both solvent and salt chemistry. Another key observation lies in the different fate of the fluorine element chemically bound to the concerned salts: in similar burning conditions, F from $NaPF_6$ decomposition is preferably converted in F-containing solid species in the residues whilst $LiPF_6$ gives off more gaseous species such as HF.

## 1. Introduction

The overutilization of fossil fuels is responsible for the greenhouse effect, the atmospheric increase in carbon dioxide levels, air and water pollution, and global warming [1]. Shifting away from fossil fuels and using renewable energy sources contribute to a carbon-neutral society [2]. The active components in lithium-ion batteries are directly not fabricated from renewable energy resources but by extracting raw materials from natural ores or in the case of sodium from brine deposits [3]. However, compared to traditional renewable energy sources, lithium-ion and sodium-ion based battery technologies remain the best compromises to provide clean stored energy on demand. The high energy and power density Li-ion batteries (LiBs) are predominantly used in electric energy accumulation devices proposed in the automobile

* Corresponding author.
*E-mail address:* guy.marlair@ineris.fr (G. Marlair).

https://doi.org/10.1016/j.jpowsour.2024.235234
Received 11 June 2024; Received in revised form 31 July 2024; Accepted 12 August 2024

industry (EVs, HEVs, and PHEVs), and portable electronics market. It is also used in grid energy storage systems (in competition to energy accumulation in hydroelectric form with pumped hydroelectric power, mechanical form with compressed air, or in electrochemical form in sodium-sulfur and redox flow batteries) [4–6]. As for sodium-ion batteries (SiBs), they have recently become a commercially available option for powering portable electronic devices.

The accidental risk linked to high-performance batteries lies in the thermal runaway hazard potentially occurring from electrical (overcharging, internal short circuits), thermal (self-heating, external heating), or mechanical (mechanical crushing) abuse or poor mishandling of batteries. Depending on the battery (electro)chemistry, a series of undesirable chemical and electrochemical reactions may take place during the thermal runaway such as the breakdown of the SEI layer, the electrolyte decomposition, the separator meltdown, the oxygen release from layered cathodes, and so on [7–10]. The increasing temperature inside the battery pack resulting from the thermal runaway reactions is accompanied by electrolyte-driven toxic gas releases, jet flames, and explosion at worst [11].

A nonaqueous electrolyte used in commercial batteries is based on a lithium or sodium salt dissolved in a mixture of organic carbonate solvents. Cyclic carbonates like ethylene and propylene carbonate (EC, PC) have high dielectric constant but with high viscosity, so that linear carbonates like dimethyl, ethyl methyl, and diethyl carbonate (DMC, EMC and DEC) must be added to lower the overall viscosity of the electrolyte [12]. The inherent flammability (Table ST1) of such electrolytes remains a critical concern for rechargeable batteries [13]. Hence, the fire behavior of electrolytes is important information for the safety assessment of the full value chain of commercial batteries. Although the solvent bases in both LiB and SiB technologies are similar and combustion tests on LiB electrolytes were already widely investigated [14,15], information on Na salts and specific additives interactions in the overall behavior of SiB electrolytes in fire conditions has not been addressed to our knowledge so far.

Therefore, this paper aims to understand the thermal (HRR, complete and effective heats of combustion, mass loss rates) and chemical threats (toxic gases) of advanced Na-ion electrolytes and compare these threats, according to close similarity in terms of composition to a classical carbonate-based electrolyte for lithium-ion batteries.

The fire hazards have been evaluated using a fire calorimeter, called Fire Propagation Apparatus (FPA) or Tewarson calorimeter in Europe [16,17], to disclose information on the potential thermal and chemical threats pertaining to fire scenarios of any combustible materials on the full spectrum of fire ventilation conditions. Description, working principle and validation domains of this bench-scale fire testing apparatus are covered by various American and international standards like NFPA 287, ASTM E2058, and ISO 12136 [18–20]. It is worth mentioning that, in the present case of burning electrolytes, obtained results only partially support what would result in a more complex situation where the electrochemical or chemical decomposition of the electrolyte would occur when inserted in a sealed battery under thermal runaway. Nevertheless, this initial study provides a good overview of the thermal and chemical threats to be assessed. The existing information on the fire behavior of lithium-ion battery electrolytes [14,15] would help create a benchmark of comparison between these analogous technologies.

## 2. Experimental

Different electrolyte formulations listed in Table 1 were prepared in a dry room with a dew point of −50 °C. EC, PC, and DMC solvents with a purity of 99.9 % were purchased from Solvionic, $NaPF_6$ salt from Stella Chemifa Corporation, NaFSI from Arkema, additives like succinonitrile (SN) from Acros Organics, vinylene carbonate (VC) and tris(trimethylsilyl) phosphite (TMSPi) from TCI Chemicals, and sodium difluorooxalatoborate (NaODFB) from E-Lyte Innovations. The chemicals are drawn in Fig. S1.

**Table 1**
Designation and composition of studied electrolytes.

| Electrolyte designation | Solvent mixture | Salt(s) | Additives |
|---|---|---|---|
| LP30 | EC/DMC (1:1 wt ratio) | $LiPF_6$ 1 mol $L^{-1}$ | |
| NP30 | EC/DMC (1:1 wt ratio) | $NaPF_6$ 1 mol $L^{-1}$ | |
| E1 | EC/PC/DMC (1:1:2 wt ratio) | $NaPF_6$ 1 mol $L^{-1}$ | |
| E1+X | EC/PC/DMC (1:1:2 wt ratio) | $NaPF_6$ 1 mol $L^{-1}$ | 3 % VC, 0.2 % TMSPi, 0.5 % NaODFB, 3 % SN |
| E2 | EC/PC/DMC (1:1:2 wt ratio) | $NaPF_6$ 0.66 mol $L^{-1}$, NaFSI 0.33 mol $L^{-1}$ | |
| E2+X | EC/PC/DMC (1:1:2 wt ratio) | $NaPF_6$ 0.66 mol $L^{-1}$, NaFSI 0.33 mol $L^{-1}$ | 3 % VC, 0.2 % TMSPi, 0.5 % NaODFB, 3 % SN |

The fire experiments were carried out in a customized version of the fire propagation apparatus as depicted in Fig. 1. The INERIS FPA is a flow through type of fire calorimeter consisting of two main subsystems. The lower part integrates the combustion chamber which accommodates the electrolyte sample (around 50 mL) placed in a Petri dish of 67 mm in diameter enclosed inside a quartz tube. The pre-weighed test sample is ignited by a pilot flame. Additionally, it is thermally heated by four infrared heaters (tungsten filament tubular quartz lamps) with an impacting external heat flux of 25 kW $m^{-2}$ on the sample surface. This acts as a non-intrusive thermal aggression, evenly radiating onto the sample surface, mocking up the impact of thermal load resulting from thermal radiation induced by established fire conditions of the test material. Well-ventilated and under-ventilated conditions corresponding to oxygen-rich and oxygen-lean environments were supplied with an incoming air-flow of 350 L $min^{-1}$ and 30 L $min^{-1}$ respectively. Obtained fire ventilation mode prevailing in each test run was verified by the calculation of the equivalence ratio also known as the phi factor (Φ) which is the ratio of fuel mass flux to the air mass flux normalized by the same parameters under stoichiometric conditions [21]. The phi value of $\Phi < 1$, $= 1$, and $>1$ refers to oxygen-rich (fuel-lean), stoichiometric, and oxygen-lean (fuel-rich) fire scenarios, respectively.

In the upper part of the calorimeter (the fire gases collector and exhaust subsystem), the fire products are captured, diluted, mixed with ambient air and further conveyed in the sampling duct, where the gas temperature and the product air-flow rate are measured. The gases were quantified in real-time using in-situ analysis for $O_2$ (paramagnetic analyzer), CO and $CO_2$ (non-dispersive infrared (NDIR) analyzers), total hydrocarbons (THC) (flame ionization detector (FID)) and soot (optical measurement). The supplementary FTIR apparatus quantified information regarding gases like carbonates, CO, $CO_2$, HCHO, $CH_4$, $C_2H_2$, $C_2H_4$, HF, $POF_3$, $SO_2$, and NO. $SiF_4$ gas originating from HF reaction with the glass quartz tube composed of $SiO_2$ was also detected and considered in the quantification of HF.

The X-Ray Diffraction (XRD) characterization of solid residues after combustion was carried out using Bruker D8 X-ray Diffractometer with Cu $K_\alpha$ radiation in the 2θ range 10–90° with subsequent step size of 0.027°. The obtained XRD peaks were analyzed and compared to standards from the International Center for Diffraction Data ($NaPF_6$ PDF #491738, NaF PDF #361455, LiF PDF #040857), with assigned power diffraction files. The chemical composition of obtained solid residues was characterized by Scanning Electron Microscopy (SEM, FEI Quanta 200-FEG) and Energy Dispersive X-ray Spectroscopy (EDX).

## 3. Results and discussion

Flaming combustion was readily achieved in all tests on the two

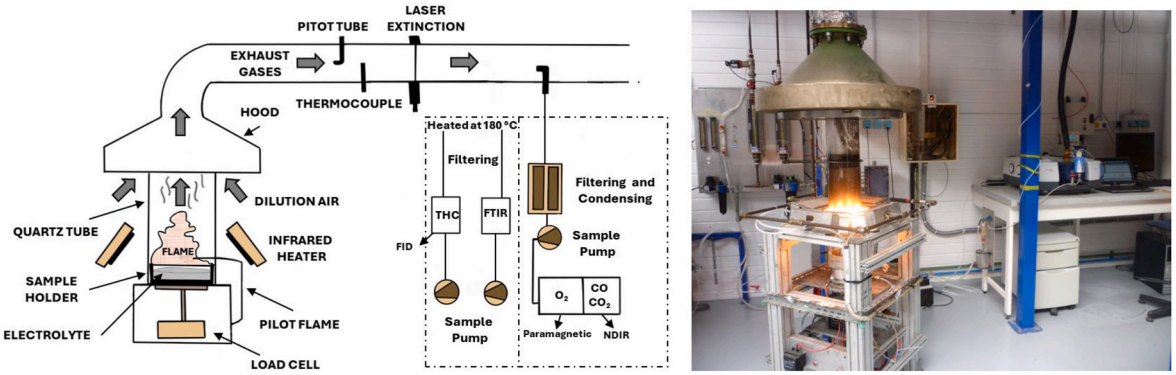


**Fig. 1.** Schematic view (left) of the FPA at INERIS and the working device pictorial representation (right).

carbonate mixtures and six electrolyte samples (Table 1) due to ease of ignition of the solvent mixtures. These electrolytes will be called basic electrolytes for LP30 and NP30 and advanced electrolytes for E1, E1+X, E2 and E2+X, whose compositions are depicted in Table 1. Note that the LP30 electrolyte composed of EC:DMC (1:1 wt ratio) solvents with 1 M $LiPF_6$ salt has been the reference electrolyte commonly used in research laboratories since 1993 [22]. EC solvent plays a significant role in the formation of passivation solid electrolyte interphase (SEI) layer on anode [23] and DMC solvent reduces the high viscosity of cyclic carbonate solvents [24]. This formulation was beforehand investigated as a reproducibility test to check whether the HRR profile and the effective heat of combustion were comparable with those obtained in a previous study from Eshetu, G.G. et al. [15]. The results were close enough to pursue our investigation using the same protocol, with confidence. The comparison of thermal and toxic gas effluents released from Ref. [15] and this study is shown in Table ST2, which validates good reproducibility of LP30 electrolyte testing in the FPA used in both studies. PC is included in the standard Na electrolyte solvent formulations [25,26]. It is an attractive solvent for low temperature operation [27], because of its low melting point (about −48.8 °C), which can lower the eutectic point of solvent with EC and thus the freezing point of the electrolyte. The synergistic mixture of $NaPF_6$ and NaFSI salts have been proven to work efficiently in sodium-ion batteries. Fan et al. [28] improved the rate capability of $NaNi_{1/3}Fe_{1/3}Mn_{1/3}O_2$||HC Na-ion cells by employing this salt mixture in a wide temperature range. NaFSI salt possesses higher conductivity [29] and $NaPF_6$ salt passivates aluminium current collector, both working as the dual salt functional electrolyte. The additives are added to stabilise the Cathode Electrolyte Interphase (CEI) and Solid Electrolyte Interphase (SEI) layer and further to improve the rate capability of $Na_3V_2(PO_4)_2F_3$||HC cells [25,26,30]. SN due to its strong nucleophilic character (-C ≡ N bond) stabilizes the high oxidation state of $V^{5+}$ to minimize parasitic reaction associated with the electrolyte [31,32]. It avoids vanadium dissolution and protects the cathode NVPF structure. TMSPi is used as an effective acid-like $HF/O_2$ scavenger [33–35], it generates a small amount of $POF_3$ and TMSF gas in the first cycle, but reduces $CO_2$ production [25]. In NVPF||HC full cell, NaODFB additive reduces the production of ethylene and hydrogen gases, while $CO_2$ and DMC-derived gaseous species were absent [36]. Hence, it contributes to the formation of stable SEI and protects the HC surface. VC additive undergoes catalytic polymerisation upon reduction and forms poly(VC)-enriched SEI layer [37–39] protecting the anode surface. In addition, VC addition is also shown to stabilise the positive NVPF electrode by forming a stable CEI layer [25].

Data on heat release rate, effective heat of combustion, gaseous emissions and solid residues obtained under well and under-ventilated fire conditions have been analyzed and discussed in the following subsections with the aim of extracting key observations about the contribution of the solvents, salts and additives in the overall combustion process. The objective was the establishment of heat and mass balances allowing the comparative assessment of the thermal and chemical threats of Li-ion and Na-ion electrolytes.

### 3.1. Heat release rate (HRR)

The HRR calculations were conducted using the principles of carbon dioxide (integrating CO and soot) generation (CDG) and oxygen consumption (OC) calorimetry techniques, the former being linked to combustion thermochemistry and the latter being based on the so-called Thornton's principle [40–42]. Both methods lead to identical and reproducible results (Fig. S2), which rely on the generic energy constant and direct mass balance conversion considering several assumptions [14,40].

*HRR profile of basic electrolytes.* As shown in Fig. 2a and b, respectively LP30 and NP30, and carbonate mixtures, EC/DMC 1:1 wt ratio and EC/PC/DMC 1:1:2 wt ratio, the HRR profiles recovered in a well-ventilated condition are divided into two distinct regions of

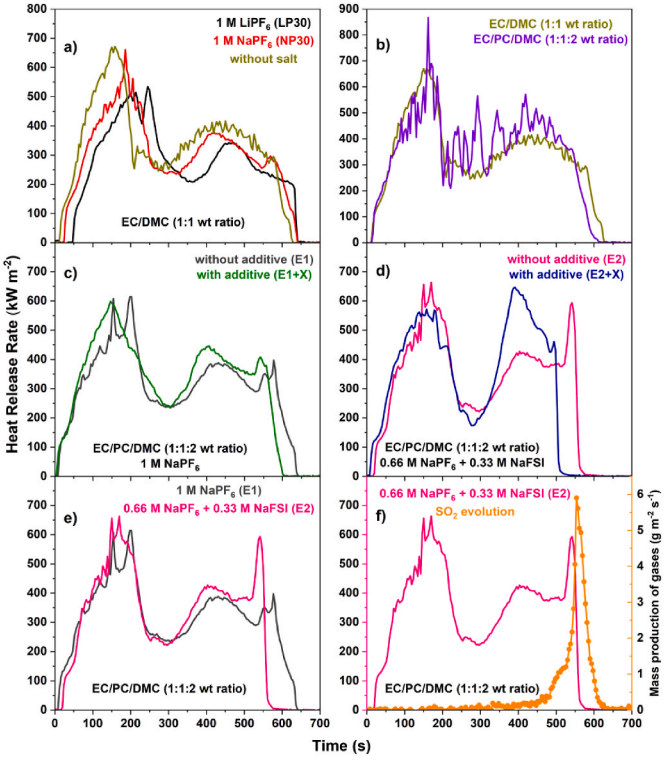


**Fig. 2.** a-e) HRR profiles of solvent mixtures and electrolytes studied under oxygen-rich environment, f) HRR profile of electrolyte E2 and related $SO_2$ gas evolution.

combustion. The latter were interpreted that the HRR of cyclic carbonate(s) follows that of linear carbonate, i.e., DMC burns faster than EC or PC due to its lower boiling point (Table ST1). Hence, the nature of the solvents mainly dictates the kinetics of energy release and their interaction (solvation) with lithium or sodium salts does not lead to any significant change in the HRR. Only a slight difference relies in the appearance of a small hump at the end of the second region of the NP30 HRR profile whereas that of the LP30 tends to decrease more gradually. The substitution of EC by PC solvent in Fig. 2b gives sharp fluctuations in HRR profile, whereas the two solvents burning individually record fairly smooth and similar results almost until the end of combustion [14]. This fluctuation might be due to the co-interaction of cyclic carbonates and their closeness in boiling points (EC ~ 247 °C, PC ~ 240 °C). It is not pronounced at the beginning of combustion mainly pertaining to DMC evaporation (0–100 s) but becomes more prominent as temperature increases. It gradually decreased at the end of the combustion (500–600 s) which suggests only one cyclic solvent is still burning.

As seen in Fig. 3, LP30 and NP30 electrolytes record a similar two-region HRR profile in the under-ventilated condition. However, the duration and the maximum intensity (as further discussed in subsection 3.3.1.1) are higher in oxygen-rich than oxygen-lean environment, the latter clearly favoring incomplete combustion. Partial oxidation of solvents occurs, which in turn produces less energy and less energy feedback reradiated to sample surface. Hence, the lower air-flow entails weaker HRR values.

*HRR profile of advanced electrolytes*. These electrolytes were investigated to test the safety impact of co-salts and the additives, VC, TMSPi, SN and NaODFB, used to improve the battery capacity retention and rate capability [25,43].

Overall, it can be seen that neither the addition of NaFSI as a co-salt (Fig. 2e) nor the usage of additives (Fig. 2c and d) show a significant change in HRR. All profiles are comparable to classical LP30 and NP30 electrolytes. Hence, these electrolytes could be used in sodium-ion batteries without any worse thermal threat potential impact in case of incident.

Taking a closer look at the HRR profiles in Fig. 2e, a sharp peak at the end of the second region of combustion is observed in case of electrolyte E2, this peak also appears but is less intense for electrolyte E1. This sudden peak relies on the decomposition of no longer solvated salts, at solid state for Li(Na)$PF_6$ and liquid state for NaFSI (melting point around 110 °C - Fig. S3). Therefore, the E2 pertaining more intense peak can be attributed to NaFSI (or its by-products) decomposition reaction; the concomitant release of $SO_2$ (Fig. 2f) corroborates this assumption. As revealed from TG measurements on salt powders (Fig. S3a), NaFSI and $NaPF_6$ decompose in a close temperature range (around 200–540 °C for NaFSI and 300–460 °C for $NaPF_6$). However, unlike $NaPF_6$ powder, whose decomposition peak is endothermic, that of NaFSI powder is exothermic with a broad peak from around 200 to 490 °C. $SO_2$ gas is only released from 410 to 490 °C (Figure S3 c, d and e) suggesting a complex thermal decomposition process. It can be assumed that the exothermic reaction triggers sudden residual solvent vaporization and combustion, explaining the sharp HRR peak as well as the earlier fire extinction as compared to the other electrolytes E1, NP30, and LP30 (560 against 610–660 s of combustion time, Table 2). The use of additives in electrolytes also decreases the time of combustion (minus 20–50 s), which might also hint that at least one of the additives undergoes an exothermic decomposition process as it is the case for instance with the salt NaODFB between 300 and 400 °C (Fig. S4).

### 3.2. *Effective heat of combustion ($\Delta Hc^{ef}$)*

The complete heat of combustion was theoretically predicated by Boie's model [44] developed in the following equation (1).

$$\Delta H_c\,(kJ\,kg^{-1}) = 35.160\,C + 116.225\,H - 11.090\,O + 6.280\,N + 10.465\,S \quad (1)$$

where C, H, O, N, and S are the mass fractions of carbon, hydrogen, oxygen, nitrogen, and sulfur in the burning analyte. The choice of this predictive method originally developed for solid fuels like coals has been made by other type of Quantitative Structure Property Relationship (QSPR) models [45], because of its widest use and recognized robustness, including from complex chemicals like ionic liquids [46]. Carbonate-based electrolytes constituting solvents, salts, and additives might follow minimal deviation from Boie's heat of combustion because descriptors in this correlation do not integrate Li, P, and F elements. Nevertheless, as reported in the literature, it works well with Li-ion electrolytes within an acceptable error range [14,15]. The integration of the HRR profile gives the experimentally obtained effective heat of combustion. Two values based on CDG and OC calorimetry were obtained which lie close to each other, and the average of the values was taken for calculating energy conversion efficiencies (Table 2).

*Oxygen-rich environment.* The values obtained for solvent mixtures and all the electrolytes range between 89 and 109 %, which might lead to the hypothesis that they all lie within Boie's model with a relative error bar of ±10 %. However, low amounts of CO, soot and THC compounds were formed, unveiling the combustion was only approaching completeness. The effective heat of combustion of the advanced electrolytes is similar to the classical NP30 electrolyte, which hints that one could use these electrolytes from a thermal menace perspective.

*Oxygen-lean environment.* The effective heat of combustion of LP30 and NP30 electrolytes is lower when tested in oxygen-lean environments (LP30: ca. 91 % vs. 75 %, NP30: ca. 103 % vs. 92 %) which relies on the lack of oxygen present to fully oxidize the carbonates. Interestingly, despite similar under-ventilated conditions, the combustion efficiency of the Na-ion electrolyte (NP30) is higher than that of the parent Li-ion

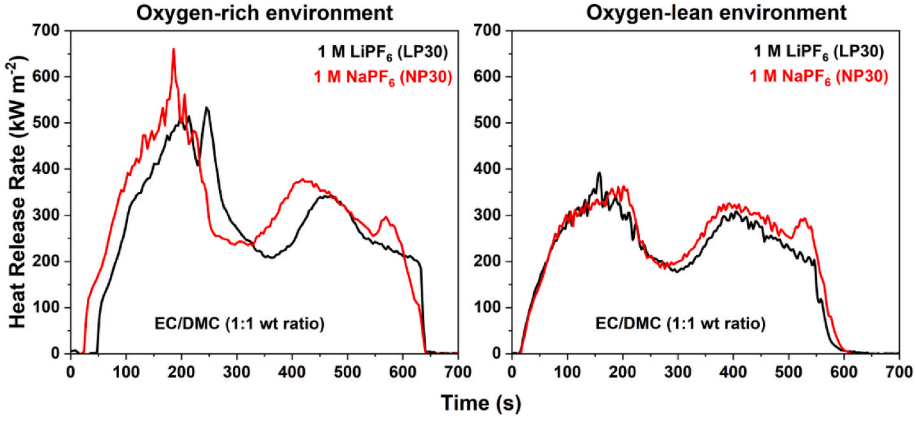


**Fig. 3.** Comparison of HRR profiles of LP30 and NP30 electrolytes in oxygen-rich and oxygen-lean environments.

**Table 2**
Thermal and chemical quantification of gases released from tested electrolytes. Data based on two independent experiments. (Last two columns: under-ventilated environment).

| | EC/DMC | EC/PC/DMC | LP30 | NP30 | E1 | E1+X | E2 | E2+X | LP30 | NP30 |
|---|---|---|---|---|---|---|---|---|---|---|
| Residue (wt. %) | 0 | 0 | 1.70 ± 0.04 | 10.30 ± 0.01 | 10.80 ± 0.05 | 9.80 ± 0.15 | 8.10 ± 0.15 | 6.80 ± 0.47 | 1.88 ± 0.20 | 9.70 ± 0.22 |
| Ease of ignition (s) | | | | | | | | | | |
| Time of combustion | 615 ± 5 | 600 | 630 ± 20 | 655 ± 5 | 650 | 600 | 560 | 525 ± 15 | 560 ± 40 | 600 |
| Heat of combustion (kJ/g of sample) | | | | | | | | | | |
| Complete heat of combustion based on Boie's model | 13.6 | 14 | 12 | 11.9 | 12.2 | 12.5 | 12.1 | 12.5 | 12 | 11.9 |
| Effective heat of combustion based on the OC method | 12.9 ± 0.2 | 15.21 ± 0.81 | 11.00 ± 0.36 | 12.0 ± 0.3 | 12.40 ± 1.09 | 13.5 ± 0.3 | 12.10 ± 0.56 | 12.5 ± 0.3 | 9.44 ± 0.21 | 10.96 ± 0.04 |
| Effective heat of combustion based on the CDG method | 12.89 ± 0.01 | 14.05 ± 0.02 | 10.78 ± 0.05 | 12.57 ± 0.01 | 13.50 ± 0.09 | 13.50 ± 0.05 | 12.80 ± 0.36 | 12.50 ± 0.14 | 8.56 ± 0.20 | 10.91 ± 0.33 |
| Average value of heat of combustion | 12.9 ± 0.1 | 14.60 ± 0.37 | 10.90 ± 0.14 | 12.30 ± 0.17 | 12.90 ± 0.54 | 13.50 ± 0.17 | 12.40 ± 0.51 | 12.50 ± 0.22 | 9 | 10.9 ± 0.2 |
| Energy conversion efficiency (%) | 95.1 ± 1.1 | 104.2 ± 3.2 | 90.5 ± 1.5 | 103.4 ± 2.4 | 105.8 ± 4.8 | 108.5 ± 0.5 | 102.6 ± 3.4 | 100.5 ± 2.5 | 74.8 ± 0.1 | 91.95 ± 1.55 |
| Product yields (mg gas/g of sample) loss | | | | | | | | | | |
| $CO_2$ | 1406 ± 5 | 1476 ± 2 | 1174 ± 6 | 1351 ± 21 | 1405 ± 14 | 1406 ± 1 | 1363 ± 10 | 1330 ± 14 | 904 ± 20 | 1163 ± 36 |
| CO | 0.6 | 0.6 ± 0.1 | 3.8 ± 0.7 | 1.2 ± 0.1 | 1.2 ± 0.1 | 2.2 ± 0.2 | 1.1 ± 0.1 | 1.9 | 65.35 ± 2.05 | 58.3 ± 1.3 |
| Soot | 1.0 ± 0.1 | 1.5 ± 0.4 | 10.8 ± 3.7 | 2.4 ± 0.6 | 4.1 ± 0.2 | 1.6 ± 0.4 | 1.8 ± 0.2 | 2.8 ± 1.5 | 11.35 ± 2.45 | 3.1 ± 0.1 |
| THC | 0.3 ± 0.3 | 0.4 ± 0.1 | 7.7 ± 1.2 | 1.8 ± 0.2 | 1.6 ± 0.1 | 1.1 ± 0.1 | 1.5 | 2.7 ± 0.2 | 26.25 ± 1.85 | 12.85 ± 0.65 |
| $CH_4$ | 0 | 0 | 0 | 0 | 0 | 0 | 0 | 0 | 5.7 ± 0.2 | 6.1 |
| $C_2H_2$ | 0 | 0 | 0 | 0 | 0 | 0 | 0 | 0 | 1.0 ± 0.2 | 0.75 ± 0.15 |
| $C_2H_4$ | 0 | 0 | 0 | 0 | 0 | 0 | 0 | 0 | 1.6 | 1.6 |
| HCHO | 0 | 0 | 0 | 0 | 0 | 0 | 0 | 0 | 1.75 ± 0.05 | 0.7 ± 0.5 |
| Overall C conversion yield in % | 95.3 ± 0.7 | 100.7 ± 0.7 | 93.4 ± 0.6 | 94.6 ± 1.6 | 99.4 ± 1.4 | 98.7 ± 0.3 | 99.5 ± 0.5 | 97.8 ± 0.2 | 85.55 ± 1.95 | 91.35 ± 1.95 |
| HF (HF + $SiF_4$) | 0 | 0 | 59.1 ± 0.7 | 16.5 ± 0.5 | 13.6 ± 0.1 | 25.5 ± 0.5 | 22.9 ± 0.9 | 33.3 ± 2.0 | 45.8 ± 2.4 | 15.95 ± 2.05 |
| $POF_3$ | 0 | 0 | 25.5 ± 1.1 | 1.2 ± 0.1 | 1.0 ± 0.1 | 7.3 ± 0.6 | 11.1 ± 0.9 | 18.4 ± 1.4 | 35.2 ± 7.9 | 1.95 ± 0.65 |
| F conversion efficiency in % (HF, $SiF_4$, $POF_3$) | – | – | 80.8 ± 0.2 | 17.3 ± 0.3 | 13.8 ± 0.2 | 28.4 ± 0.4 | 38 ± 2 | 56.3 ± 4.3 | 72.05 ± 2.35 | 17.35 ± 2.55 |
| P conversion efficiency in % ($POF_3$) | – | – | 59.2 ± 2.8 | 2.5 ± 0.5 | 2.1 ± 0.1 | 15 ± 1 | 35.7 ± 2.7 | 59.4 ± 4.4 | 81.55 ± 18.35 | 4.25 ± 1.35 |
| $SO_2$ | 0 | 0 | 0 | 0 | 0 | 0 | 19.6 ± 0.5 | 27.2 ± 1.5 | 0 | 0 |
| Fuel-S to $SO_2$ conversion efficiency (%) | – | – | – | – | – | – | 55.3 ± 1.3 | 77.8 ± 4.8 | – | – |
| NO | 0 | 0 | 0 | 0 | 0 | 2.8 ± 0.1 | 1.4 ± 0.2 | 3.2 ± 0.1 | 0 | 0 |
| Fuel-N to N-containing emissions conversion efficiency in % | – | – | – | – | – | 13.9 ± 0.1 | 17.2 ± 1.8 | 10 | – | – |

electrolyte (LP30), with the latter releasing higher levels of CO, soot and THC. The lower thermal stability and higher sensitivity to hydrolysis of $LiPF_6$ compared to $NaPF_6$ (due to the bigger and less polarizing sodium cation than the lithium cation) can be incriminated. Indeed, in both cases, emitted HF quantities increase during the combustion process but the LP30 electrolyte gives off more HF than the NP30 (Fig. 4). The gas production whose chemical reactions are detailed in the gas analysis subsection (3.3.2) tends to limit $O_2$ diffusion from the air to the fuel, resulting in a less complete combustion reaction.

### 3.3. Gaseous emission analysis

The fire propagation apparatus permits qualifying and quantifying in real-time the gases generated by combustion of electrolytes in fire conditions. These gases emitted from solvents and salts/additives used in the electrolyte account for the chemical threat according to the resulting toxicity/corrosivity potential [47]. As the fate of chemical products could change with fire ventilation conditions, gases formed from LP30 and NP30 electrolytes were carefully examined in both oxygen-rich and lean environments.

#### 3.3.1. Gases coming from solvents

*3.3.1.1. LP30 and NP30 electrolytes. In oxygen-rich environment.* As shown in Table 2 for both LP30 and NP30 electrolytes, a close-to-complete combustion is revealed from energy conversion efficiency calculation. This is favored by oxygen containing species in the electrolyte and easy diffusion of oxygen from the air in the developing

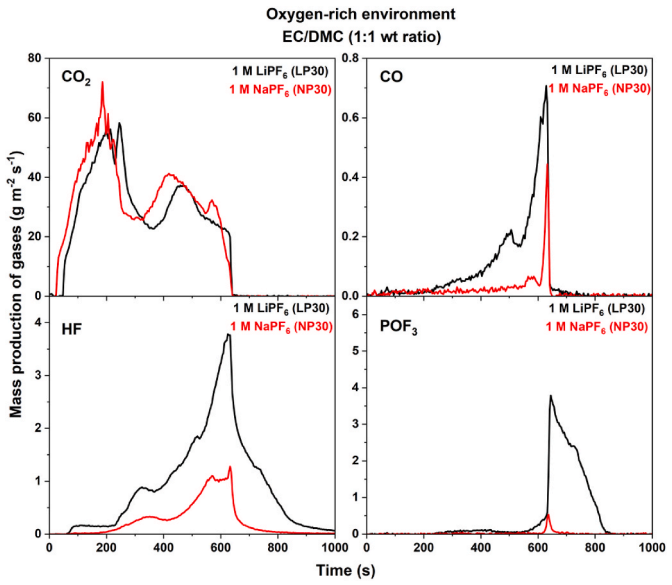


**Fig. 4.** Gases released during combustion of LP30 and NP30 electrolytes under oxygen-rich environment.

diffusion flames. As a result, $CO_2$ (Fig. 4) and water vapor are the major gaseous products, which is of no serious concern in terms of toxicity. For both electrolytes, poisonous CO gas is also generated in very limited quantities mainly at the end of the second stage of combustion (EC burning region); LP30 generates about 3 times more CO than NP30 (ca. 3.8 *vs.* 1.2 mg of CO emitted/g of LP30 and NP30 resp.). As explained hereafter, $LiPF_6$ decomposes faster than $NaPF_6$ salt and forms more HF and fluorophosphates which most likely slightly hamper locally the efficiency of the mixing process of oxygen and solvent vapours in our test conditions. This creates a pseudo-oxygen lean environment forming some more CO and other unburnt species (soot, THC) thus also globally slightly diminishing the overall combustion efficiency.

*In oxygen-lean environment.* As can be seen for LP30 and NP30 in Fig. 5, the $CO_2$ peak intensity reached during the first region pertaining to dimethyl carbonate combustion is lower than in oxygen-rich environment whereas the difference is less significant in the second region

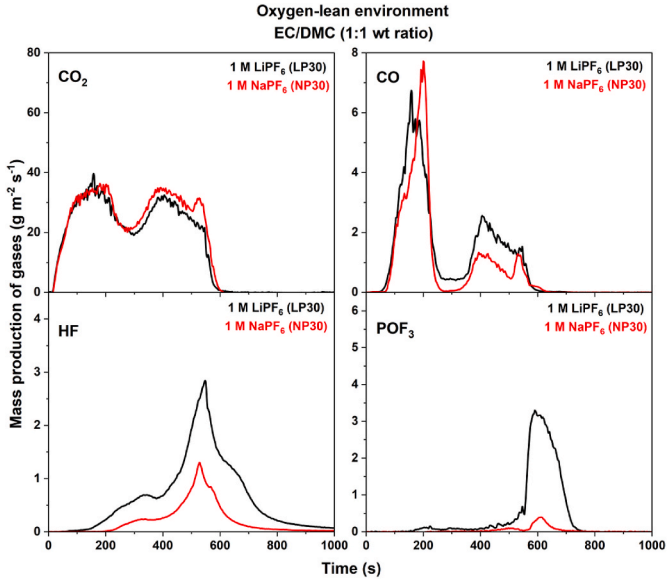


**Fig. 5.** Gases released during combustion of LP30 and NP30 electrolytes under oxygen-lean environment.

pertaining to ethylene carbonate combustion. On the other hand, unlike tests carried out in oxygen-rich environment where CO is mainly produced at the end of the combustion process, CO is released from the beginning in oxygen-lean environment, in two distinct regions; intensity is much more pronounced in the first region than in the second. Both $CO_2$ and CO production profiles can be explained by the too high vaporization rate of the DMC solvent; oxygen quantity and diffusion rate into the flame are insufficient, resulting in a more incomplete combustion process during the first region. During the second region, the EC vaporization rate is low enough to undergo a more complete combustion.

The CO production is obviously increased in under-ventilated conditions, with LP30 still showing a little bit higher CO emission than NP30 (ca. 65 *vs.* 58 mg of CO emitted/g of electrolyte). The difference is not that much significant, however, in each scenario relating to a given application of SiBs, a deeper analysis would be needed to see how far toxicity of SiB fires proceeding in under-ventilated mode would foster the CO driven toxicity risk. Maybe large fires involving SiBs storage in fire resistant structures would make some difference.

Table 2 shows that additional hydrocarbons like formaldehyde, ethylene, ethyne, and methane gases were produced in small quantities during under-ventilated fires due to incomplete combustion of electrolytes. Such gases were absent in a well-ventilated atmosphere where almost complete combustion into $CO_2$ and $H_2O$ occurs.

*3.3.1.2. Advanced Na-ion electrolytes.* Similar to classical electrolytes, tests carried out in well-ventilated conditions reveal that they produce $CO_2$ and CO (Figs. 6 and 7) accounting for the major conversion products of elemental carbon chemically bound in the solvents. As previously observed with LP30 and NP30 electrolytes, adding salts (E1 and E2) to the solvent mixture (EC/PC/DMC) results in favoring more incomplete combustion, i.e., pure solvents give off higher $CO_2$ emission than the electrolytes with salts (Table 2). Overall, with or without salts, $CO_2$ is released in two stages, with a higher emission rate during the first stage

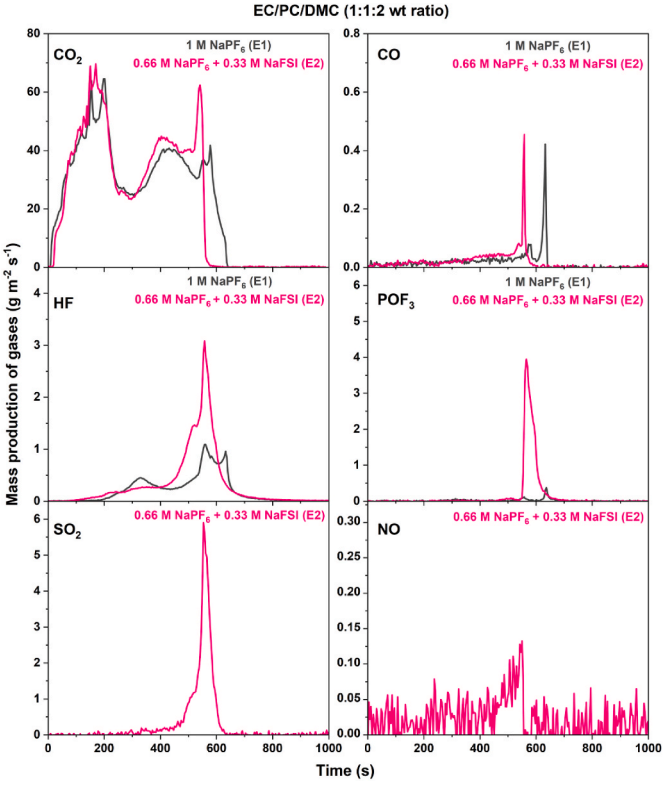


**Fig. 6.** Gases released during combustion of E1 and E2 electrolytes (effect of salt).

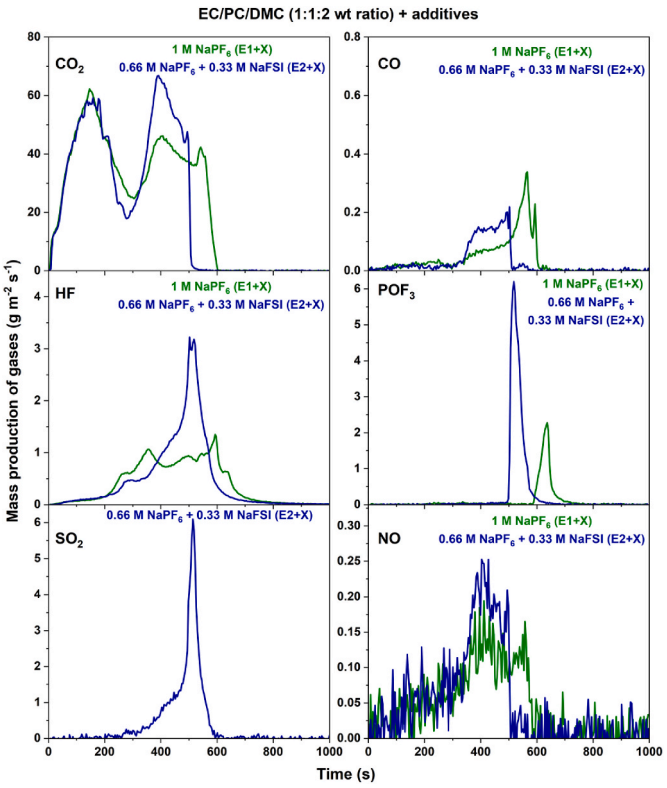


**Fig. 7.** Gases released during combustion of E1+X and E2+X electrolytes (effect of additives).

associated with linear solvents burning. The bump due to decomposition of salts at the end of the combustion is revealed earlier and more intensively when NaFSI is present (E2 electrolyte).

Concerning CO emissions, all these Na electrolytes release less amount of CO and soot than the lithium salt electrolyte (LP30), which was hereabove explained by a less thermal stability and higher sensitivity to hydrolysis of $LiPF_6$, compared to $NaPF_6$ and NaFSI.

As shown in Fig. 6, not only do electrolytes E1 and E2 show a similar CO production profile with a sharp peak (like NP30) at the end of the second phase of combustion but they also generate equivalent amounts of CO (Table 2).

The presence of additives as shown in Fig. 7 results in a reduction in the combustion time and a little bit increase of the CO production (ca. 2.2 *vs.* 1.2 and 1.9 *vs.* 1.1 mg/g of E1+X/E1 and E2+X/E2, respectively).

The $CO_2$ and CO production profiles are also altered in presence of additives; it is noteworthy that, from the start of the second stage, the $CO_2$ and CO production stemming from burning NaFSI-based electrolyte (E2+X) exhibits a marked increase in comparison to E2, whereas the difference is hardly visible in the case of E1 and E1+X. This suggests that an exothermic reaction involving NaFSI and an additive occurs during the second stage of combustion, therefore increasing the EC vaporization rate.

### 3.3.2. Gases coming from salts

*3.3.2.1. LP30 and NP30 electrolytes.* As shown in Figs. 4 and 5 and quantitatively represented in Table 2, NP30 generates significantly lesser HF and $POF_3$ than LP30 electrolyte in both well and under ventilated conditions. This is a quite remarkable and robust result, largely confirmed by the analysis of the mass balance establishment as regard the fluorine element (section 3.5). A relatively same amount of HF and $POF_3$ released in both ventilation conditions suggests that their production is not much affected by the combustion process intensity. Indeed, the fate of $LiPF_6$ and $NaPF_6$ salts is likely to result from the subsequent decomposition pathway steps: i) the thermal decomposition of Li(Na)$PF_6$ (when dissolved in solvents or in solid state at the end of the combustion process) leading to $PF_5$ and Li(Na)F (Eqs. (2) and (3)) and ii) the hydrolysis of the $PF_5$ gas in the combustion chamber to form HF and $POF_3$, according to previously published results [48]. It is interesting to note that, for all tested electrolytes, $POF_3$ is only detected just after the carbonate burning process while HF is released earlier. This suggests that the $PF_5$ hydrolysis reaction (Eq. (4)) takes place from the water produced by the combustion process of the carbonate solvents. The reaction product $POF_3$, in turn, undergoes subsequent hydrolysis reactions to yield other not detected compounds as $HPO_2F_2$, $H_2PO_3F$ and $H_3PO_4$ along with additional HF (Eqs. (5)–(7)). After combustion, $PF_5$ hydrolysis still occur but there is not enough water in the chamber to enable hydrolysis of the $POF_3$, which is therefore detected along with HF.

$$LiPF_6\ (s) \rightarrow LiF\ (s) + PF_5\ (g) \quad (2)$$

$$NaPF_6\ (s) \rightarrow NaF\ (s) + PF_5 \quad (3)$$

Hydrolysis reactions:

$$PF_5 + H_2O \rightarrow 2HF + POF_3\ (g) \quad (4)$$

$$POF_3 + H_2O \rightarrow HF + HPO_2F_2\ (g \text{ at } T > 116\ ^\circ C) \quad (5)$$

$$HPO_2F_2 + H_2O \rightarrow HF + H_2PO_3F \quad (6)$$

$$H_2PO_3F + H_2O \rightarrow HF + H_3PO_4 \quad (7)$$

As $NaPF_6$ is much more stable to thermal decomposition and hydrolysis than $LiPF_6$ which is evidenced by their decomposition temperature (Figs. S3a, b, c) starting at around 320 and 125 °C respectively [49], NP30 electrolyte generates fewer quantities of HF and $POF_3$ than LP30 electrolyte.

*3.3.2.2. Advanced Na-ion electrolytes.* As shown in Fig. 6 and Table 2, HF emissions increase more with electrolyte E2 than E1 (ca. 23 vs. 14 mg of HF emitted/g of E2 and E1, respectively). A similar trend is observed for $POF_3$ gas generation where emissions increase about 11 times more with electrolyte E2 than E1 (ca. 11 vs. 1 mg of $POF_3$ emitted/g of E2 and E1, respectively). Considering the HRR profiles, assumption was put forward above that the exothermic thermal decomposition of NaFSI at the end of the second stage is at the origin of sudden cyclic solvent vaporization and combustion peak. This phenomenon impacts the thermal decomposition of $NaPF_6$ and $PF_5$ hydrolysis reactions in contact with water vapor, thereby increasing the production of HF along with $POF_3$. Following fire tests carried out with LiFSI electrolyte [15], hydrolysis of the NaFSI salt and/or its thermal degradation compounds could also be considered as a supplementary source of HF emission during combustion tests. Indeed, Zhou et al. [50] proposed an $FSI^-$ hydrolysis reaction path releasing HF:

$$2N(FSO_2)_2^- + 4H_2O \rightarrow FSO_2NH_2 + NH_2SO_3^- + FSO_3^- + SO_4^{2-} + 2HF + 2H^+$$

It is worth noting that all thermal degradation compounds are not well identified yet, indeed authors agree that a more detailed investigation is needed to fully understand the decomposition mechanisms in wet and dry conditions. Although NaFSI is more stable than LiFSI, we took an interest in decomposition pathways of heated neat LiFSI already investigated in literature using mass spectrometry. Huang et al. [51] detected at only 180 °C, prominent peaks at *m/z* 48 ($SO^+$), 64 ($SO_2^+$), 89 ($LiSO_2F^+$), −180 ($N(SO_2F)_2^-$), −367 ($Li[N(SO_2F)_2]_2^-$), −99 ($SO_3F^-$), −261 ($FSO_2NSOFNSO_2F^-$) and −342 ($FSO_2(NSFO)_2NSO_2F^-$). From the two latter fragments, they suggested the formation of $FSO_2N$ radicals. In dry conditions, they can bond with S atom in a fragment containing the $FSO_2N^-$ group, repeatedly, to form an oligomer structure. In wet conditions, water would interrupt this process and produce non identified small fragments. Hong-Bo Han et al. [52] detected $SO_2$ and $NO_2$ as main

gaseous products released upon heating up to higher temperature (550 °C) and obtained 31 wt% of the initial mass in the solid residue that cannot correspond to a singly pure LiF phase (13.9 wt%).

The addition of additives to electrolytes E1 and E2 results in an increase in the emission of HF and $POF_3$, as observed in Table 2, which remains inferior to that of $LiPF_6$-based electrolyte. This suggests that exothermic reactions involving additives may occur, leading to higher thermal reactivity and hydrolysis of $NaPF_6$. Indeed, from hereabove solvent combustion gas analysis, it was assumed that, from the beginning of the second stage, NaFSI might undergo an exothermic thermal reaction with at least one additive, leading to enhanced emission of all gas emitted from carbonate combustion, $NaPF_6$ and additive decomposition but also from NaFSI such as NO and $SO_2$ (Figs. 6 and 7). It is worth discussing that in such temperature conditions, there is no chance to develop thermal $NO_x$ by oxidation of $N_2$ from air, due to Zeldovitch mechanism [53]. In our case, only N-fuel may be partially converted in N-containing species: state of the art as regard the fate of N-fuel in fires considers that a main part would convert into $N_2$, whilst in well-ventilated conditions, some fraction (generally below 10 % for liquids) would be converted in $NO_x$ (essentially NO). In our case, the only sources of fuel-N are SN additive and NaFSI. NO was detected in extremely minute quantities (ca. 2.8, 1.4 and 3.2 mg of NO/g of E1+X, E2 and E2+X, resp.) to be related to limited nitrogen concentration in tested electrolytes and moderate conversion ratios (Table 4) usually encountered from combustion of N-containing organic materials. Note that, as N-containing materials are generally favored to form $N_2$ in fire conditions and since 78 % of the air-flow comprises nitrogen, the conversion efficiency of N during combustion cannot be calculated with certainty. As for the fate of S element, NaFSI containing electrolytes E2 and E2+X gave off either detected $SO_2$ as a gaseous product or S-containing solid product(s) in the residues detected by EDX but not yet identified by XRD, as shown in Fig. 8.

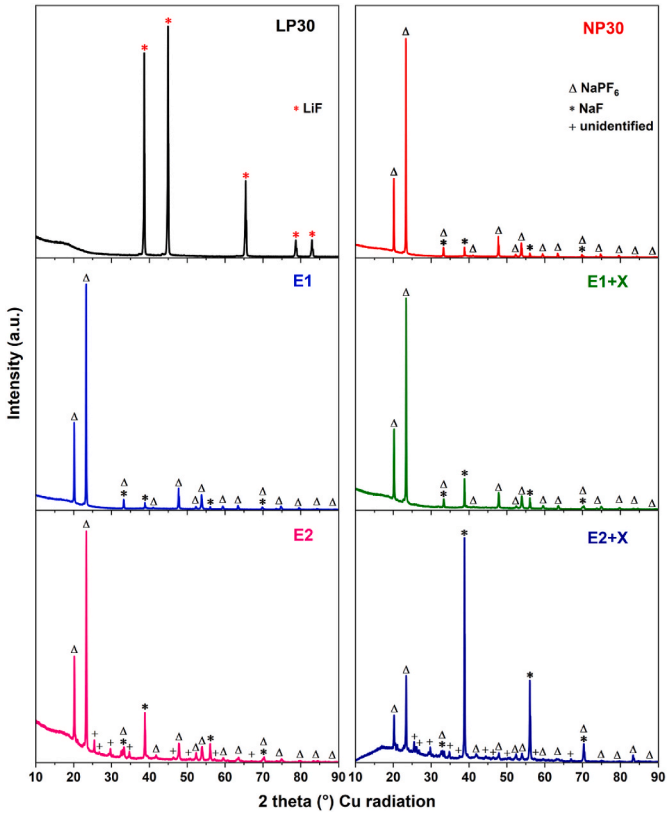


**Fig. 8.** XRD patterns of tested electrolyte residues.

### 3.4. Combustion products: XRD and EDX analysis of solid residues

After combustion, LP30, NP30 and E1 gave off a greyish-white colored residue while electrolytes E1+X, E2 and E2+X gave off a black-colored solid residue. In the latter electrolytes, a peak corresponding to the C element is clearly visible by EDX, so it is assumed that the black color is due to a small amount of soot left in the residues. A higher amount of solid residue (4–6 times more) was left behind in the case of sodium electrolytes (NP30, E1, E1+X, E2 and E2+X) compared to classical lithium electrolyte LP30. From the XRD analysis (Fig. 8), the residue is composed solely of LiF for LP30 and both $NaPF_6$ and NaF phases for NP30, E1 and E1+X as shown in Fig. 8, corroborating the higher thermal stability of $NaPF_6$. EDX results in Table 3 shows that for LP30 residue, >99 wt% of the elemental composition contribution come from LiF with minute phosphorus traces. On the other hand, NP30 and E1 residues were composed of around 8 more times of $NaPF_6$ than NaF and E1+X, of around 2.5 more time. E2 and E2+X electrolytes, left $NaPF_6$, NaF, and some unidentified peaks resulting from NaFSI salt as supported by EDX analysis that shows the presence of N and S elements (Table 3). Note that the presence of N in E1+X residue reveals that it can also stem from the decomposition of the additive SN.

### 3.5. Mass balance and the fate of key elements forming tested electrolyte

The elemental mass balance calculations were achieved for each element recovery ratio [54,55]. It is defined as the ratio of the total amount of that element measured in fire effluents in the form of all the gaseous releases and in the mass residue, to the amount of that initial element before combustion. A conversion efficiency of 100 % would be expected in an ideal case. Within experimental uncertainties, results presented in Table 4 are globally in good agreement with the exception of N (conversion of around 20–35 %) which, in addition to NO, is suspected of recombining into $N_2$, P (conversion >60 %) which is suspected of being in undetected $HPO_2F_2$, $H_2PO_3F$ or $H_3PO_4$ species and Na (for electrolytes with additives: conversion of around 75 %) for which, honestly, there is no chemical explanation.

Despite of real difficulties in measuring F gaseous species, the mass balance as regard F element is very good in all tests. During combustion, fluorine gets converted into Li(Na)F residues and gaseous products such as HF ($SiF_4$ after subsequent reaction with glass) and $POF_3$ that may subsequently be hydrolyzed into $HPO_2F_2$, $H_2PO_3F$ and $H_3PO_4$. Regarding LP30 electrolyte, it is worth noticing that 81 % of fluorine gets converted into gases while around 19 % exists in residues. From these outcomes, it is safe to assume that almost all $LiPF_6$ decompose into LiF (19 % exp. against 17 % calc.) and $PF_5$. Since the fluorine conversion yield is total, we can postulate that the 5 fluorine of $PF_5$ are converted into 38 % ($H_3PO_4$ + 5 HF) and 62 % ($POF_3$ + 2 HF). The presence of the intermediate compounds, $HPO_2F_2$ and $H_2PO_3F$, would have led to a non-total F conversion yield, so they were not formed. It is worth recalling that hydrolysis reactions of $PF_5$ into $H_3PO_4$ are allowed owing to the water released from the combustion reaction of carbonate solvents. After extinction, as the air-flow is dry, there is just enough water left in the chamber for the hydrolysis reaction to result in $POF_3$. This means that in the event of a real fire, $POF_3$ could still undergo hydrolysis

**Table 3**
EDX analysis of tested electrolyte residues. (Error calculated from 3 analysis points).

| Element (wt%) | LP30 | NP30 | E1 | E1+X | E2 | E2+X |
|---|---|---|---|---|---|---|
| F | 99.7 ± 0.1 | 64 ± 4 | 65 ± 4 | 50 ± 4 | 42 ± 3 | 44 ± 3 |
| P | 0.3 ± 0.1 | 19 ± 2 | 19 ± 2 | 13 ± 2 | 9 ± 1 | 12 ± 1 |
| Na | | 16 ± 2 | 15 ± 2 | 14 ± 2 | 20 ± 2 | 19 ± 2 |
| O | | | 2 ± 1 | 4 ± 1 | 9 ± 2 | 8 ± 2 |
| C | | | | 17 ± 2 | 9 ± 1 | 8 ± 1 |
| N | | | | 2 ± 1 | 3 ± 1 | 2 ± 1 |
| S | | | | | 7 ± 1 | 7 ± 1 |

**Table 4**
Elemental mass balance: Element releases versus original sample.

| Conversion (%) | LP30 | | | NP30 | | | E1 | | | E1+X | | | E2 | | | E2+X | | |
|---|---|---|---|---|---|---|---|---|---|---|---|---|---|---|---|---|---|---|
| | Gases | Residue | Total | Gases | Residue | Total | Gases | Residue | Total | Gases | Residue | Total | Gases | Residue | Total | Gases | Residue | Total |
| C | 93.4 ± 0.6 | 0 | **93** | 94.6 ± 1.6 | 0 | **95** | 99.4 ± 1.4 | 0 | **99** | 98.7 ± 0.3 | 5 | **104** | 99.5 ± 0.5 | 2 | **102** | 97.8 ± 0.2 | 2 | **100** |
| F | 80.8 ± 0.2 | 19 | **100** | 17.3 ± 0.3 | 79 | **96** | 13.8 ± 0.2 | 79 | **93** | 28.4 ± 0.4 | 56 | **84** | 38 ± 2 | 51 | **89** | 56.3 ± 4.3 | 47 | **103** |
| N | – | – | **-** | – | – | **-** | – | – | **-** | 13.9 ± 0.1 | 16 | **30** | 17.2 ± 1.8 | 16 | **33** | 10 | 11 | **21** |
| S | – | – | **-** | – | – | **-** | – | – | **-** | – | – | **-** | 55.3 ± 1.3 | 38 | **93** | 77.8 ± 4.8 | 33 | **111** |
| P | 59.2 ± 2.8 | 0.2 | **59** | 2.5 ± 0.5 | 87 | **90** | 2.1 ± 0.1 | 84 | **86** | 15 ± 1 | 55 | **70** | 35.7 ± 2.7 | 50 | **86** | 59.4 ± 4.4 | 54 | **113** |
| Na | – | – | **-** | 0 | 99 | **99** | 0 | 90 | **90** | 0 | 75 | **75** | 0 | 96 | **96** | 0 | 74 | **74** |

reaction with the moisture from the ambient air to release the additional products, HF and $H_3PO_4$.

Due to the higher stability of Na salts, the inverse conversion is observed for NP30 and E1 as well as it only differs by the solvent composition; 14–17 % of fluorine gets converted into gases while around 79 % exists in residues. Besides, $POF_3$ is released in very small quantity leading to P-gas conversion percentage of around 2 %. Hence, we can say that, as far as HF emissions are concerned, NP30 represents a much smaller chemical threat than LP30, even in the event of a real fire. This further supports the safety argument of sodium-ion batteries, which suggests that during thermal runaway, the electrolyte would mostly convert into residue and release fewer toxic chemical gases.

It is worth noting that using additives and substituting $NaPF_6$ by NaFSI tends to increase F and P-gas conversion %. Anyway, since NaFSI contains only 2 F and some $NaPF_6$ was found to be left in solid residue, the HF emission-related threat will never reach that of LP30 and NP30. However, it must be considered that NaFSI induces $SO_2$ irritant gas release with 55 and 78 conversion %, the residual S element remaining in the solid residue.

### 3.6. Global discussion

The HRR profiles of both carbonate solvent mixtures and hexafluorophosphate-based electrolytes were found to be almost similar depicting two regions linked to the subsequent combustion of the linear then cyclic carbonates in line with their boiling point. Besides, combustion efficiencies in a well-ventilated condition were found to approach 100 % which was expectable because low molecular significantly oxygenated species are known in literature to burn efficiently [56]. They were however slightly lower than 100 % for solvents mixtures and slightly over 100 % for electrolytes, which can be explained by the fact that the Boie predictive model of complete heat of combustion was not originally developed for battery electrolyte samples (only C, H, O, N, S descriptors in the model, whilst other elements are present in the test electrolytes). Additionally, some errors may also originate from the calculation of the effective heats of combustion, since the accuracy of OC and relating CDG principle used to perform these calculations can vary according to test scale and complexity of the burning molecules [41,57]. Obviously, under-ventilated conditions lower the combustion effectiveness and thus increase the carbon monoxide emission principally in the first region because of the fast evaporation of linear carbonate.

These results highlight the importance of finding safer electrolyte solvents in terms of better reaction-to-fire-properties, that are compatible with the development of next-generation high-energy density and power sodium-ion batteries. Endeavors are devoted to introducing flame-retardant additives or solvents [58,59] presenting inherent flame retarding properties (like ionic liquids) into the electrolytes generally resulting in compromised battery performance because of their inefficiency to undergo cation de-solvation process or passivate carbonaceous anodes. Salt-concentrated electrolytes [60] can resolve this issue by forming a robust inorganic SEI and participate in the cation coordination sphere. Interestingly, in recent years, researchers have highlighted the significant influence of the cation solvation structures in the design of high-performance and reported 'non-flammable' electrolytes with lower salt concentrations and flame-retardant solvent [61], based for instance on lithium difluoro(oxalato)borate (LiDFOB) additive in the mixture of dimethoxyethane (DME) solvent and hydrofluoroether (HFE) diluent [62], trimethyl phosphate [63], and fluorinated ester and cyclophosphazene with high flame retardancy efficiency [64].

Based on this concept, the impact of cation-solvent interactions on the combustion process is worth discussing. It can be assumed that the strong $Li^+$ (or $Na^+$)-EC interaction (due to the high donor number of EC) would impede the evaporation of the solvent and therefore the combustion process. However, in this electrolyte combustion scenario, DMC and increasing amount of EC (and PC) first evaporate, hence, the electrolyte becomes increasingly concentrated in Li salt and ends up

behaving like an ionic liquid. An anion is therefore expected to appear in the first solvation shell due to insufficient solvent, effectively weakening the $Li^+$-solvent interaction. This would promote EC solvent evaporation and thus explain the similarity in the second region of the solvent mixtures and electrolytes' HRR profiles.

Li(Na)$PF_6$ salts have a significant impact on the amount of toxic gases emitted as products of their thermal degradation and hydrolysis reactions, preferably after solvent exhaustion. Based on the qualitative HSAB theory, the softer $Na^+$ acid has a more stable interaction with the soft $PF_6^-$ base than its $Li^+$ counterpart. $NaPF_6$ is thus more thermally stable than $LiPF_6$ and, unlike $LiPF_6$, tends to remain intact in residue after combustion. The $PF_5$ formed from the thermally degraded part of the salt can be subjected to successive hydrolysis reactions to produce between two and five undesirable hydrofluoric acid (HF) molecules, depending on the water content from the carbonate combustion reactions or available in the ambient air. Given the above, $NaPF_6$ represents a much lesser chemical threat than $LiPF_6$, a very good news according to the ever-lasting debate on the genuine threat of F-containing species and relating fire toxicity impact in case of battery fire events.

The introduction of NaFSI into the electrolyte causes an additional thermal and chemical threat at the end of the combustion owing to its sudden exothermic decomposition. This initiates a cascade of subsequent degradation processes, including the evaporation and combustion of the remaining cyclic solvent molecules and the greater extent of $NaPF_6$ decomposition. All these reactions generate an increase in the quantity of toxic gases (irritant HF and $SO_2$, and asphyxiant CO). NaFSI may also react with additives as observed in the present study through the more intense and shortened second region of the HRR profile. Unfortunately, the thermal degradation mechanisms of NaFSI in the presence of water and additives are not elucidated and would deserve deeper investigations. More importantly, due to the release of the various toxic gases HF, $SO_2$ and NO, the threat of fire-induced toxicity in the event of a major cell failure at different states of charge should be assessed on the basis of experimental data and the technical use of international fire safety standards [65].

## 4. Conclusion

The fire behavior of carbonate-based lithium and sodium electrolytes was studied using the Fire Propagation Apparatus (FPA). Accurate online gas quantification provided valuable data on thermal (HRR and effective heat of combustion) and chemical threats (toxic gas emission). All electrolytes exhibited a two-region solvent-dominated heat release rate profile with very little differences depending on the nature of the salt. Only NaFSI-induced decomposition reactions with/without additives and ventilation conditions demonstrated to impact its intensity and shape, mainly at the end of combustion.

A difference in the production of toxic and hazardous CO, HF and $POF_3$ gases was observed when comparing hexafluorophosphate electrolytes due the higher thermal stability and stability toward hydrolysis of $NaPF_6$ salt as compared to $LiPF_6$. Some of the less reactive $NaPF_6$ remains in the residues after combustion, while up to 5–6 of the fluorine atoms in $LiPF_6$ are likely to be released in the form of HF and phosphates.

Even if carbonate-based electrolytes for sodium-ion batteries hint at the increased safety over conventional Li-ion electrolyte, further full-level investigations on cell and module level must also to be planned to confirm the observed safety gain as more complex electrolytes thermal decomposition and oxidation reactions would be likely to occur through interacting with active materials such as $O_2$-fuel releasing layered cathode materials.

## CRediT authorship contribution statement

**Pempa Tshering Bhutia:** Writing – original draft, Visualization, Investigation, Formal analysis. **Sylvie Grugeon:** Writing – review & editing, Validation. **Jean-Pierre Bertrand:** Visualization, Formal analysis, Data curation. **Ghislain Binotto:** Visualization, Resources, Data curation. **Arnaud Bordes:** Writing – review & editing. **Asmae El Mejdoubi:** Validation, Resources. **Stéphane Laruelle:** Validation, Supervision, Project administration, Formal analysis. **Guy Marlair:** Writing – review & editing, Validation, Supervision, Project administration, Conceptualization.

## Declaration of competing interest

The authors declare that they have no known competing financial interests or personal relationships that could have appeared to influence the work reported in this paper.

## Data availability

Data will be made available on request.

## Acknowledgments

As a part of the DESTINY PhD program, this publication is acknowledged by funding from the European Union's Horizon2020 research and innovation program under the Marie Skłodowska-Curie Actions COFUND (Grant Agreement #945357). We thank Loic Dupont, Jennifer Bidal, TIAMAT team and Nikhil Subash and for technical help. We also thank Aurélie Aube for her assistance in the thermal analysis and relating plots of additives and salts reported in supplementary information sheet.

## Appendix A. Supplementary data

Supplementary data to this article can be found online at https://doi.org/10.1016/j.jpowsour.2024.235234.

## References

[1] N. Armaroli, V. Balzani, The legacy of fossil fuels, Chem. Asian J. 6 (2011) 768–784, https://doi.org/10.1002/asia.201000797.
[2] L. Chen, G. Msigwa, M. Yang, A.I. Osman, S. Fawzy, D.W. Rooney, P.-S. Yap, Strategies to achieve a carbon neutral society: a review, Environ. Chem. Lett. 20 (2022) 2277–2310, https://doi.org/10.1007/s10311-022-01435-8.
[3] M. Armand, J.-M. Tarascon, Building better batteries, Nature 451 (2008) 652–657, https://doi.org/10.1038/451652a.
[4] B. Dunn, H. Kamath, J.-M. Tarascon, Electrical energy storage for the grid: a battery of choices, Science 334 (2011) 928–935, https://doi.org/10.1126/science.1212741.
[5] B. Diouf, R. Pode, Potential of lithium-ion batteries in renewable energy, Renew. Energy 76 (2015) 375–380, https://doi.org/10.1016/j.renene.2014.11.058.
[6] T. Chen, Y. Jin, H. Lv, A. Yang, M. Liu, B. Chen, Y. Xie, Q. Chen, Applications of lithium-ion batteries in grid-scale energy storage systems, Trans. Tianjin Univ. 26 (2020) 208–217, https://doi.org/10.1007/s12209-020-00236-w.
[7] C. Zu, H. Yu, H. Li, Enabling the thermal stability of solid electrolyte interphase in Li-ion battery, InfoMat 3 (2021) 648–661, https://doi.org/10.1002/inf2.12190.
[8] X. Xu, X. Cheng, F. Jiang, S. Yang, D. Ren, P. Shi, H. Hsu, H. Yuan, J. Huang, M. Ouyang, et al., Dendrite-accelerated thermal runaway mechanisms of lithium metal pouch batteries, SusMat 2 (2022) 435–444, https://doi.org/10.1002/sus2.74.
[9] H. Kondou, J. Kim, H. Watanabe, Thermal analysis on Na plating in sodium ion battery, Electrochemistry 85 (2017) 647–649, https://doi.org/10.5796/electrochemistry.85.647.
[10] X. Tian, Y. Yi, B. Fang, P. Yang, T. Wang, P. Liu, L. Qu, M. Li, S. Zhang, Design strategies of safe electrolytes for preventing thermal runaway in lithium ion batteries, Chem. Mater. 32 (2020) 9821–9848, https://doi.org/10.1021/acs.chemmater.0c02428.
[11] P. Sun, R. Bisschop, H. Niu, X. Huang, A review of battery fires in electric vehicles, Fire Technol. 56 (2020) 1361–1410, https://doi.org/10.1007/s10694-019-00944-3.
[12] D. Monti, E. Jónsson, A. Boschin, M.R. Palacín, A. Ponrouch, P. Johansson, Towards standard electrolytes for sodium-ion batteries: physical properties, ion solvation and ion-pairing in alkyl carbonate solvents, Phys. Chem. Chem. Phys. 22 (2020) 22768–22777, https://doi.org/10.1039/D0CP03639K.
[13] A. Swiderska-Mocek, P. Jakobczyk, E. Rudnicka, A. Lewandowski, Flammability parameters of lithium-ion battery electrolytes, J. Mol. Liq. 318 (2020) 113986, https://doi.org/10.1016/j.molliq.2020.113986.

[14] G.G. Eshetu, S. Grugeon, S. Laruelle, S. Boyanov, A. Lecocq, J.-P. Bertrand, G. Marlair, In-depth safety-focused analysis of solvents used in electrolytes for large scale lithium ion batteries, Phys. Chem. Chem. Phys. 15 (2013) 9145, https://doi.org/10.1039/c3cp51315g.

[15] G.G. Eshetu, J.-P. Bertrand, A. Lecocq, S. Grugeon, S. Laruelle, M. Armand, G. Marlair, Fire behavior of carbonates-based electrolytes used in Li-ion rechargeable batteries with a focus on the role of the LiPF6 and LiFSI salts, J. Power Sources 269 (2014) 804–811, https://doi.org/10.1016/j.jpowsour.2014.07.065.

[16] C. Costa, G. Treand, F. Moineault, J.-L. Gustin, Assessment of the thermal and toxic effects of chemical and pesticide pool fires based on experimental data obtained using the Tewarson apparatus, Process Saf. Environ. Protect. 77 (1999) 154–164, https://doi.org/10.1205/095758299529974.

[17] G. Marlair, F.H. Prager, H. Sand, The behaviour of commercially important di-isocyanates in fire conditions Part 1: toluene di-isocyanate (TDI), Fire Mater. 17 (1993) 91–102, https://doi.org/10.1002/fam.810170206.

[18] NFPA 287, STANDARD TEST METHODS FOR MEASUREMENT OF FLAMMABILITY MATERIALS IN CLEANROOMS USING A FIRE PROPAGATION APPARATUS (FPA), 2022. ISBN 978-1-4559-2849-1.

[19] ASTM E 2058-19 Standard Test Methods for Measurement of Material Flammability Using a Fire Propagation Apparatus (FPA).

[20] ISO 12136:2011, Reaction to Fire Tests — Measurement of Material Properties Using a Fire Propagation Apparatus, 2011.

[21] A. Tewarson, Ventilation effects on combustion products, Toxicology 115 (1996) 145–156, https://doi.org/10.1016/S0300-483X(96)03503-2.

[22] D. Guyomard, J.M. Tarascon, Rechargeable Li1 + x Mn2 O 4/carbon cells with a new electrolyte composition: potentiostatic studies and application to practical cells, J. Electrochem. Soc. 140 (1993) 3071–3081, https://doi.org/10.1149/1.2220987.

[23] A. Wang, S. Kadam, H. Li, S. Shi, Y. Qi, Review on modeling of the anode solid electrolyte interphase (SEI) for lithium-ion batteries, npj Comput. Mater. 4 (2018) 15, https://doi.org/10.1038/s41524-018-0064-0.

[24] M.S. Ding, K. Xu, T.R. Jow, Liquid-solid phase diagrams of binary carbonates for lithium batteries, J. Electrochem. Soc. 147 (2000) 1688, https://doi.org/10.1149/1.1393419.

[25] P. Desai, J. Huang, H. Hijazi, L. Zhang, S. Mariyappan, J. Tarascon, Deciphering interfacial reactions via optical sensing to tune the interphase chemistry for optimized Na-ion electrolyte formulation, Adv. Energy Mater. 11 (2021) 2101490, https://doi.org/10.1002/aenm.202101490.

[26] P. Desai, J. Forero-Saboya, V. Meunier, G. Rousse, M. Deschamps, A.M. Abakumov, J.-M. Tarascon, S. Mariyappan, Mastering the synergy between Na3V2(PO4)2F3 electrode and electrolyte: a must for Na-ion cells, Energy Storage Mater. 57 (2023) 102–117, https://doi.org/10.1016/j.ensm.2023.02.004.

[27] L. Chen, J. Shu, Y. Huang, Z. Shi, H. Luo, Z. Liu, C. Shen, Engineering solid electrolyte interphase for the application of propylene carbonate solvent for graphite anode in low temperate battery, Appl. Surf. Sci. 598 (2022) 153740, https://doi.org/10.1016/j.apsusc.2022.153740.

[28] W. Fan, W. Wang, Q. Xie, X. He, H. Li, J. Zhao, J. Nan, A sodium bis (Fluorosulfonyl)Imide (NaFSI)-based multifunctional electrolyte stabilizes the performance of $NaNi_{1/3}Fe_{1/3}Mn_{1/3}O_2$/hard carbon sodium-ion batteries, Chem. Eur J. (2024) e202401321, https://doi.org/10.1002/chem.202401321.

[29] L.M. Kha, V.D. Thanh, N. Van Hoang, L.V. Thang, L.M.L. Phung, Electrochemical performance of hard carbon anode in different carbonate-based electrolytes, Vietnam Journal of Chemistry 58 (2020) 643–647, https://doi.org/10.1002/vjch.202000053.

[30] G. Yan, K. Reeves, D. Foix, Z. Li, C. Cometto, S. Mariyappan, M. Salanne, J. Tarascon, A new electrolyte formulation for securing high temperature cycling and storage performances of Na-ion batteries, Adv. Energy Mater. 9 (2019) 1901431, https://doi.org/10.1002/aenm.201901431.

[31] G.-Y. Kim, J.R. Dahn, The effect of some nitriles as electrolyte additives in Li-ion batteries, J. Electrochem. Soc. 162 (2015) A437–A447, https://doi.org/10.1149/2.0651503jes.

[32] Y.-S. Kim, T.-H. Kim, H. Lee, H.-K. Song, Electronegativity-induced enhancement of thermal stability by succinonitrile as an additive for Li ion batteries, Energy Environ. Sci. 4 (2011) 4038, https://doi.org/10.1039/c1ee01272j.

[33] Y.-K. Han, J. Yoo, T. Yim, Why is tris(trimethylsilyl) phosphite effective as an additive for high-voltage lithium-ion batteries? J. Mater. Chem. A 3 (2015) 10900–10909, https://doi.org/10.1039/C5TA01253H.

[34] T. Yim, S.-G. Woo, S.H. Lim, W. Cho, J.H. Song, Y.-K. Han, Y.-J. Kim, 5V-Class high-voltage batteries with over-lithiated oxide and a multi-functional additive, J. Mater. Chem. A 3 (2015) 6157–6167, https://doi.org/10.1039/C4TA06531J.

[35] Y.-M. Song, J.-G. Han, S. Park, K.T. Lee, N.-S. Choi, A multifunctional phosphite-containing electrolyte for 5 V-class $LiNi_{0.5}Mn_{1.5}O_4$ cathodes with superior electrochemical performance, J. Mater. Chem. A 2 (2014) 9506–9513, https://doi.org/10.1039/C4TA01129E.

[36] L. Zhang, C. Tsolakidou, S. Mariyappan, J.-M. Tarascon, S. Trabesinger, Unraveling gas evolution in sodium batteries by online electrochemical mass spectrometry, Energy Storage Mater. 42 (2021) 12–21, https://doi.org/10.1016/j.ensm.2021.07.005.

[37] A.L. Michan, BharathyS. Parimalam, M. Leskes, R.N. Kerber, T. Yoon, C.P. Grey, B. L. Lucht, Fluoroethylene carbonate and vinylene carbonate reduction: understanding lithium-ion battery electrolyte additives and solid electrolyte interphase formation, Chem. Mater. 28 (2016) 8149–8159, https://doi.org/10.1021/acs.chemmater.6b02282.

[38] K.U. Schwenke, S. Solchenbach, J. Demeaux, B.L. Lucht, H.A. Gasteiger, The impact of $CO_2$ evolved from VC and FEC during formation of graphite anodes in lithium-ion batteries, J. Electrochem. Soc. 166 (2019) A2035–A2047, https://doi.org/10.1149/2.0821910jes.

[39] S. Grugeon, P. Jankowski, D. Cailleu, C. Forestier, L. Sannier, M. Armand, P. Johansson, S. Laruelle, Towards a better understanding of vinylene carbonate derived SEI-layers by synthesis of reduction compounds, J. Power Sources 427 (2019) 77–84, https://doi.org/10.1016/j.jpowsour.2019.04.061.

[40] W.M.X.V. Thornton, The relation of oxygen to the heat of combustion of organic compounds, London, Edinburgh Dublin Phil. Mag. J. Sci. 33 (1917) 196–203, https://doi.org/10.1080/14786440208635627.

[41] H. Biteau, A. Fuentes, G. Marlair, S. Brohez, J.L. Torero, Ability of the fire propagation apparatus to characterise the heat release rate of energetic materials, J. Hazard Mater. 166 (2009) 916–924, https://doi.org/10.1016/j.jhazmat.2008.11.100.

[42] O. Willstrand, M. Pushp, H. Ingason, D. Brandell, Uncertainties in the use of oxygen consumption calorimetry for heat release measurements in lithium-ion battery fires, Fire Saf. J. 143 (2024) 104078, https://doi.org/10.1016/j.firesaf.2023.104078.

[43] Sathiya Mariyappan, Jean-Marie Tarascon, Hijazi Hussein, Patent Number US 2024/0178451 A1, Electrolyte Composition for Sodium-Ion Battery, 2023.

[44] K. Annamalai, W. Ryan, Interactive processes in gasification and combustion—II. Isolated carbon, coal and porous char particles, Prog. Energy Combust. Sci. 19 (1993) 383–446, https://doi.org/10.1016/0360-1285(93)90010-C.

[45] A.O. Diallo, C. Len, A.B. Morgan, G. Marlair, Revisiting physico-chemical hazards of ionic liquids, Separ. Purif. Technol. 97 (2012) 228–234, https://doi.org/10.1016/j.seppur.2012.02.016.

[46] A.-O. Diallo, G. Fayet, C. Len, G. Marlair, Evaluation of heats of combustion of ionic liquids through use of existing and purpose-built models, Ind. Eng. Chem. Res. 51 (2012) 3149–3156, https://doi.org/10.1021/ie2023788.

[47] A.-O. Diallo, A.B. Morgan, C. Len, G. Marlair, An innovative experimental approach aiming to understand and quantify the actual fire hazards of ionic liquids, Energy Environ. Sci. 6 (2013) 699, https://doi.org/10.1039/c2ee23926d.

[48] S. Solchenbach, M. Metzger, M. Egawa, H. Beyer, H.A. Gasteiger, Quantification of $PF_5$ and $POF_3$ from side reactions of $LiPF_6$ in Li-ion batteries, J. Electrochem. Soc. 165 (2018) A3022–A3028, https://doi.org/10.1149/2.0481813jes.

[49] G.G. Eshetu, S. Grugeon, H. Kim, S. Jeong, L. Wu, G. Gachot, S. Laruelle, M. Armand, S. Passerini, Comprehensive insights into the reactivity of electrolytes based on sodium ions, ChemSusChem 9 (2016) 462–471, https://doi.org/10.1002/cssc.201501605.

[50] S. Zhou, S. Zhang, S. Wang, W. Zhang, Y. Liu, H. Lin, J. Chen, L. Yan, F. Zhang, H. Li, et al., Direct evidences for bis(Fluorosulfonyl)Imide anion hydrolysis in industrial production: pathways based on thermodynamics analysis and theoretical simulation, J. Power Sources 577 (2023) 233249, https://doi.org/10.1016/j.jpowsour.2023.233249.

[51] J. Huang, A.F. Hollenkamp, Thermal behavior of ionic liquids containing the FSI anion and the $Li^+$ cation, J. Phys. Chem. C 114 (2010) 21840–21847, https://doi.org/10.1021/jp107740p.

[52] H.-B. Han, S.-S. Zhou, D.-J. Zhang, S.-W. Feng, L.-F. Li, K. Liu, W.-F. Feng, J. Nie, H. Li, X.-J. Huang, Lithium bis(Fluorosulfonyl)Imide (LiFSI) as conducting salt for nonaqueous liquid electrolytes for lithium-ion batteries: physicochemical and electrochemical properties, J. Power Sources 196 (2011) 3623–3632, https://doi.org/10.1016/j.jpowsour.2010.12.040.

[53] E.L. Merryman, A. Levy, Nitrogen oxide formation in flames: the roles of NO2 and fuel nitrogen, Symposium (International) on Combustion 15 (1975) 1073–1083, https://doi.org/10.1016/S0082-0784(75)80372-9.

[54] S. Brohez, G. Marlair, C. Delvosalle, Fire calorimetry relying on the use of the fire propagation apparatus. Part I: early learning from use in Europe, Fire Mater. 30 (2006) 131–149, https://doi.org/10.1002/fam.896.

[55] S. Brohez, G. Marlair, C. Delvosalle, Fire calorimetry relying on the use of the fire propagation apparatus. Part II: burning characteristics of selected chemical substances under fuel rich conditions, Fire Mater. 30 (2006) 35–50, https://doi.org/10.1002/fam.897.

[56] A. Tewarson, G. Marlair, in: C.A. Harper (Ed.), Liquids and Chemicals, Chapter 8, Handbook of Building Materials for Fire Protection, McGraw-Hill handbooks, McGraw-Hill: New York, 2004. ISBN 978-0-07-138891-7.

[57] S. Brohez, C. Delvosalle, G. Marlair, A. Tewarson, The measurement of heat release from oxygen consumption in sooty fires, J. Fire Sci. 18 (2000) 327–353, https://doi.org/10.1177/073490410001800501.

[58] G.G. Eshetu, S. Jeong, P. Pandard, A. Lecocq, G. Marlair, S. Passerini, Comprehensive insights into the thermal stability, biodegradability, and combustion chemistry of pyrrolidinium-based ionic liquids, ChemSusChem 10 (2017) 3146–3159, https://doi.org/10.1002/cssc.201701006.

[59] A. Yusuf, D. Wang, Toward an in-depth fire hazard and resistance diagnosis of flame retarded liquid electrolytes for safer lithium-ion batteries, Adv Materials Technologies 7 (2022) 2101055, https://doi.org/10.1002/admt.202101055.

[60] J. Wang, Y. Yamada, K. Sodeyama, E. Watanabe, K. Takada, Y. Tateyama, A. Yamada, Fire-extinguishing organic electrolytes for safe batteries, Nat. Energy 3 (2017) 22–29, https://doi.org/10.1038/s41560-017-0033-8.

[61] H. Cheng, Q. Sun, L. Li, Y. Zou, Y. Wang, T. Cai, F. Zhao, G. Liu, Z. Ma, W. Wahyudi, et al., Emerging Era of electrolyte solvation structure and interfacial model in batteries, ACS Energy Lett. 7 (2022) 490–513, https://doi.org/10.1021/acsenergylett.1c02425.

[62] Q. Sun, Z. Cao, Z. Ma, J. Zhang, W. Wahyudi, G. Liu, H. Cheng, T. Cai, E. Xie, L. Cavallo, et al., Interfacial and interphasial chemistry of electrolyte components to invoke high-performance antimony anodes and non-flammable lithium-ion batteries, Adv. Funct. Mater. 33 (2023) 2210292, https://doi.org/10.1002/adfm.202210292.

[63] H. Cheng, Z. Ma, P. Kumar, H. Liang, Z. Cao, H. Xie, L. Cavallo, Q. Li, J. Ming, Non-flammable electrolyte mediated by solvation chemistry toward high-voltage lithium-ion batteries, ACS Energy Lett. 9 (2024) 1604–1616, https://doi.org/10.1021/acsenergylett.3c02789.
[64] Y. Zou, Z. Ma, G. Liu, Q. Li, D. Yin, X. Shi, Z. Cao, Z. Tian, H. Kim, Y. Guo, et al., Non-flammable electrolyte enables high-voltage and wide-temperature lithium-ion batteries with fast charging, Angew. Chem. Int. Ed. 62 (2023) e202216189, https://doi.org/10.1002/anie.202216189.
[65] A. Lecocq, G.G. Eshetu, S. Grugeon, N. Martin, S. Laruelle, G. Marlair, Scenario-based prediction of Li-ion batteries fire-induced toxicity, J. Power Sources 316 (2016) 197–206, https://doi.org/10.1016/j.jpowsour.2016.02.090.